International Journal of Heat and Mass Transfer 129 (2019) 86–95

Contents lists available at ScienceDirect

International Journal of Heat and Mass Transfer

journal homepage: www.elsevier.com/locate/ijhmt

Dropwise condensation on superhydrophobic nanostructure surface, Part I: Long-term operation and nanostructure failure

Jian Xie [a], Jinliang Xu [a,b,*], Xiang Li [a], Huan Liu [a]

[a] Beijing Key Laboratory of Multiphase Flow and Heat Transfer for Low Grade Energy Utilization, North China Electric Power University, Beijing 102206, China
[b] Key Laboratory of Condition Monitoring and Control for Power Plant Equipment of Ministry of Education, North China Electric Power University, Beijing 102206, China

ARTICLE INFO

Article history:
Received 17 April 2018
Received in revised form 13 September 2018
Accepted 19 September 2018

Keywords:
Dropwise condensation
Superhydrophobic surface
Long-term operation
Droplet removal
Failure

ABSTRACT

Dropwise condensation heat transfer (DWC) on superhydrophobic nanograsses surface (NGS) was investigated for long-term operation. For DWC of pure water-vapor on fresh NGS, two heat transfer regimes are identified: higher heat transfer coefficients with droplet jumping, and constant heat transfer coefficients with droplet rolling. The one-week operation not only deteriorates heat transfer performance, but also changes jumping or rolling mode to sliding mode. The condensation heat transfer coefficients are apparently decreased from first to third day, but they approach a limit value since the third day. In order to identify if the single-molecule-layer of polymer (SML) modified on nanograsses was destroyed, DWC on a smooth single-molecule-layer of polymer surface (SSML) was tested to display stable heat transfer with drop sliding for one-week operation, concluding no failure of the polymer layer. The collapse and breakage of nanograsses were observed to explain the decayed heat transfer versus time on NGS. Compared with SSML, the NGS has smaller droplet departure size but lower heat transfer coefficients, indicating positive and negative effects after introducing nanostructures. Three nanostructure failure mechanisms are proposed. This work suggests a new research field of the nanoscale fluid-wall interaction.

1. Introduction

In 1930, Schmidt et al. [1] found dropwise condensation on a chrome plated copper surface. Compared with filmwise condensation, dropwise condensation can have one order of magnitude higher heat transfer coefficients. Since then, condensation heat transfer was investigated on gold or silver surface. The enhanced heat transfer is due to the surface pollution by organic substances, which is related to the surface carbon content [2–4]. Due to high cost of gold or silver material, investigators turned to coat organic substance layer on metal surface by self-organization or plasma injection techniques.

Dropwise condensation displays the cycle behavior. Each cycle contains four processes: drop nucleation, growth, coalescence and detachment [5]. After drop departure, a new cycle begins at the location that is initially occupied by the drop before departure. Among the four processes, the drop departure is key to influence heat transfer [6]. If a surface has a small contact angle hysteresis, heat transfer is improved due to the easy droplet removal. A surface with appropriate lubricant behaves low contact angle hysteresis [7,8]. A conventional method is to use the surfaces with coating layer of fluorocarbon polymer, resin, sulfuret, graphene or rare earth oxide [9–14], which are believed to satisfy the "*large contact angle and small contact angle hysteresis*" criterion.

In recent years, with fast development of micro/nano fabrication techniques, scientists are interested in various superhydrophobic nanostructure surfaces to improve dropwise condensation. Such surfaces do satisfy the "*large contact angle and small contact angle hysteresis*" criterion. However, with deep understating of dropwise condensation, such criterion is questioned. Here, we gave a brief review on the advantages of nanostructure surface first. In the environment such as moisture air, low pressure pure vapor, or small wall subcooling (low condensation heat flux), condensation heat transfer is better on nanostructure surface. Miljkovic et al. [15] demonstrated a 25% higher overall heat flux and 30% higher condensation heat transfer coefficient on nanostructure surface compared to smooth polymer surface at supersaturations less than 1.12, which is attributed to coalescence induced jumping. The self-actuated jumping yields one to two orders magnitude smaller drop departure size, compared with the sliding mode [16,17]. Zhu et al. [18] performed

* Corresponding author at: Beijing Key Laboratory of Multiphase Flow and Heat Transfer for Low Grade Energy Utilization, North China Electric Power University, Beijing 102206, China.
E-mail address: xjl@ncepu.edu.cn (J. Xu).

https://doi.org/10.1016/j.ijheatmasstransfer.2018.09.100
0017-9310/

condensation experiments in 3–7 kPa vapor environment. They showed over 125% condensation heat transfer enhancement by using nanostructure surface compared with smooth polymer surface. Not only coalescence induced jumping, but also increased drop nucleation sites account for heat transfer enhancement. Similar conclusion was drawn by Kim and Nam [19], in which they stated 60% heat transfer enhancement with nanostructure surface.

Many condensers practically operate in higher pressure/temperature environment than above. For example, the saturation pressure and temperature are above atmospheric pressure and 100 °C respectively, for pure water-vapor. Under such circumstances, nanostructure surface may not sustain long-term operation to resist surface failure. Miljkovic et al. [15] noted that when the vapor supersaturations are larger than 1.12, nanostructure surface has lower heat transfer performance than smooth polymer surface. Instead, the coalescence induced jumping mode is replaced by the shedding mode. Some surface locations are covered by liquid film to form flooding. In a following paper, they stated that the added nano-porous thermal conduction resistance is another reason to worsen heat transfer [20]. Zhang et al. [21] noted that hydrophobic surface increases the energy barrier for droplet nucleation, which also behaves a negative effect to improve DWC. For superhydrophobic nanostructure surface, Zhu et al. [18] reported decreased heat transfer enhancement factors when the saturation pressure is increased. When the saturation pressure is increased to atmospheric pressure, Lan et al. [22] showed poorer condensation heat transfer on nanostructure surface than that on smooth hydrophobic surface, who attributed the decreased free energy difference in solid-liquid-vapor phase system as the reason. Ma et al. [23] reported that, only when the non-condensable gas content is extremely large, nanostructure surface has better condensation heat transfer than smooth polymer surface. When the non-condensable gas content is decreased, nanostructure surface may not behave obvious advantages. Similar conclusion was drawn by Hu et al. [24]. These authors highlighted the importance of wetting state (Cassie, Wenzel, or partial Wenzel) on condensation heat transfer [22–24].

Zhang et al. [21] reported the decayed DWC on hydrophobic coating surface. The decayed DWC data on superhydrophobic nanostructure surface is less reported. The long-term operation changes surface topology to influence nucleation sites, contact angle, contact angle hysteresis, drop detachment and nano-porous thermal conduction resistance. Thus, heat transfer performance is altered. The analysis is not reported in the literature. The objective of this paper is to: (1) compare dropwise condensation on superhydrophobic nanograsses surface (NGS) and smooth single-molecule-layer of polymer surface (SSML); (2) analyze the changes of surface nanostructure, droplet detachment mode and heat transfer performance on NGS and SSML during one-week operation. Three nanostructure failure mechanisms are proposed in the end of this paper. The phenomenon observed in this part will be theoretically analyzed in Part II of this paper series [25].

2. The experimental setup

2.1. The experimental system

Fig. 1a shows the experimental system, including a saturation vapor supplier loop, a chiller water loop, a test sample package and a measurement system. A cooling chamber, a copper test sample and a condensing chamber were integrated to form the test sample package. The test sample had a 30.0 mm diameter and a 20.0 mm length. The test surface was vertically positioned. Parallel fins were fabricated on the left side surface, dissipating heat to the chiller water. Both the fin width and gap were 2.0 mm respectively. The right side of the test sample was the test surface. Three test samples were prepared: a hydrophilic smooth copper surface without micro/nano fabrication (SCS), a superhydrophobic nanograsses surface (NGS), and a hydrophobic smooth single-molecule-layer of polymer surface (SSML). Their fabrication processes will be described in the next section. Along the test sample axial length, three thermocouples were penetrated to the copper block centerline with a 15.0 mm depth. The first thermocouple T_1 had a 6.0 mm distance from the test surface (see Fig. 1b). The distances from T_1 to T_2, and from T_2 to T_3, were 4.0 mm. The heat conducting glue was filled between thermocouple and penetrating hole. In order to prevent heat from releasing to environment, the whole copper test sample was tightly inserted inside a Teflon cylinder. The heat insulation thickness was 15.0 mm.

Pure saturation vapor was supplied by a steam generator, which was controlled by an electric heater. Deionized water was in the steam generator bottom. A two-phase separator was in the steam generator top to prevent water droplet from entering the condensing chamber. The vapor mass flow rate was measured via a pressure drop transducer across an orifice. Before formal experiment, the relationship between pressure drop and flow rate was calibrated, while the flow rate was determined by weighing condensed water during a specific time. During experiment, the condensed water was collected and further cooled in a post-condenser. When the liquid level in the post-condenser was increased to a specific value, water was pumped to the steam generator.

Our experiment was performed at a saturation pressure of ~20 kPa, having a saturation temperature of ~60 °C. Typically, the vapor mass flow rate was m_s = 1.10 kg/h, the corresponding vapor velocity was $u \sim 3.0$ m/s over the condensing chamber cross section. Because the condensing chamber was running in vacuum pressure, the non-condensable gas effect is obvious [26]. The following procedure was performed to remove non-condensable gas: (1) The vapor supplier system was vacuumed to a 20 Pa pressure. Maintaining the 20 Pa pressure without vacuuming by 48 h concludes no system leakage. (2) Deionized water was boiled by one hour. Then, the condensed water was charged into the initially vacuumed vapor supplier system. (3) Water in the steam generator was heated to a temperature of 110.0 °C to reach the pressure of 143.4 kPa. Manual opening the safety valve of the steam generator discharged vapor to environment. The pure vapor state was ensured by examining the relationship between vapor pressure and temperature. For example, when the measured pressure is 19.9 kPa in condensing chamber, the measured temperature is 60.1 °C, which approaches the pressure determined saturation temperature of 60.0 °C.

The chiller water loop generated spray cooling to the test sample. The chiller water temperature could be adjusted in the range of 0.5–40.0 °C to reach different wall subcoolings and heat fluxes for the condenser surface. For each run, the chiller water temperature was quite stable with oscillation less than 0.5 °C. A gear pump circulated the chiller water. A nozzle generated droplets spray that was impacting on the left side surface of the test sample.

2.2. Fabrication of the test surface

The fabrication procedures are as follows.

Step 1 (base surface preparation): The copper block surface was polished by sand papers and fine diamond polishing paste consecutively. It was rinsed by acetone and methanol consecutively to remove the oil contamination. It is noted that the polishing process was performed using a rotating machine. The friction induced heat during the polishing process may generate surface oxidization. In order to ensure the surface without oxidization layer, the polished surface was further immersed in a 0.2% weight

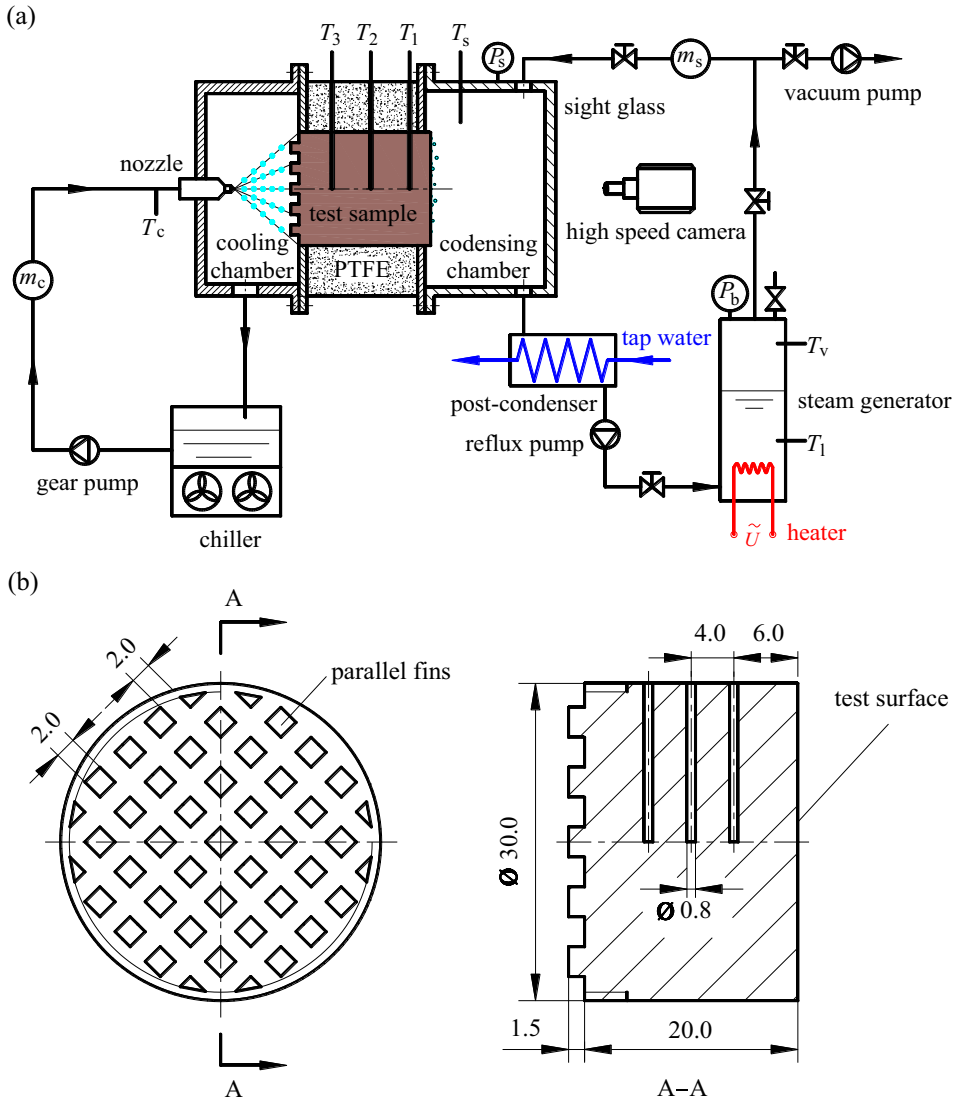

Fig. 1. The experimental setup.

concentration hydrochloric acid solution by 2 min. This step was over after the sample was rinsed by deionized water and dried by blowing nitrogen gas.

Step 2 (Alkali type wet oxidation [27,28]): A 2.5 mol/L NaOH (Aladdin, GR) solution and a 0.1 mol/L $(NH_4)_2S_2O_8$ (Aladdin, AR) solution were mixed to form a mixture solution. The sample after step 1 was in the solution for chemical reaction by 12 min. Then the sample was rinsed by deionized water and baked in an oven by 2 h. This step was over once the sample was naturally cooled to environment temperature.

Step 3 (self-organization of macromolecules layer): The sample after step 2 was immersed in a 0.5% weight concentration ethanol solution of 1H, 1H, 2H, 2H-perfluorooctyltriethoxysilane (Alfa Aesar, AR) by 2 h. Magnetic stirring having a 500 rpm rotating speed promoted the reaction to form polymer layer on the surface. The wet sample was baked in the oven by 2 h. The 50 °C baking temperature is much lower than the 69 °C boiling temperature of ethanol. Under such condition, ethanol is evaporating instead of boiling, which is helpful for self-origination of the polymer molecules on the surface.

Three test samples were prepared. The hydrophilic smooth copper surface (called SCS) followed step 1 fabrication only for filmwise condensation. The hydrophobic smooth single-molecule-layer of polymer surface (SSML) followed steps 1 and 3 fabrication. The superhydrophobic nanograsses surface (NGS) followed all the three steps fabrication.

2.3. Data reduction

Table 1 summarized measurement parameters, instruments and uncertainties. Condensation experiments were performed in the vapor environment of P_s = 20 kPa, T_s = 60 °C and u = 3 m/s. For any test surface, heat flux on the condenser surface (q) was changed by altering flow rate and temperature of chiller water impacting on the copper block cooling side. Here, q is calculated based on the three thermocouples measurements according to one-dimensional heat conduction assumption of the copper block cylinder. Such assumption is verified by testing the relationship between the three temperatures of T_1, T_2 and T_3, noting equal distance from T_1 to T_2, and from T_2 to T_3 (see Fig. 1). Fig. 2a shows that $T_1 - T_2$ is almost identical to $T_2 - T_3$. The radial heat conduction of the copper cylinder can be neglected to ensure the one-dimensional heat conduction assumption. Heat flux q is

$$q = \frac{\lambda}{L_{1-3}}(T_1 - T_3) = \frac{\lambda}{L_{1-2}}(T_1 - T_2) = \frac{\lambda}{L_{2-3}}(T_2 - T_3) \quad (1)$$

Table 1
Summary of parameters, instruments and uncertainties.

Parameters	Instruments	Uncertainties
Temperature T_1, T_2, T_3, T_c, T_s	K-type jacket thermocouple	±0.1 °C
Steam pressure P_s	Rosemount-3051 pressure transducer	±0.5%
Steam mass flow rate m_s	DMF-1-DX mass flow meter	±0.1%
Cooling water mass flow rate m_c	DMF-1-DX mass flow meter	±0.1%
Heat flux q		±2.6–6.4%
Condensation heat transfer coefficient h		±3.8–10.5%

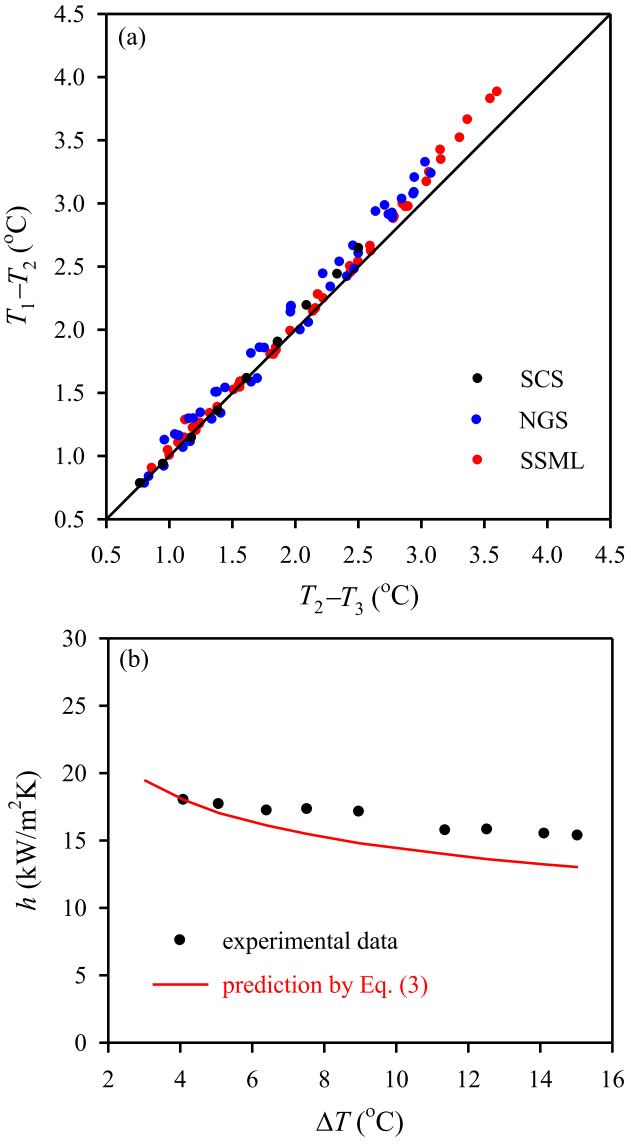

Fig. 2. Calibration experiment (a: relationship between two temperature differences; b: comparison between measured condensation heat transfer coefficients and predicted values. SCS represents hydrophilic smooth copper surface without micro/nano fabrication, NGS represents superhydrophobic nanograsses surface, SSML represents hydrophobic smooth single-molecule-layer of polymer surface).

where $\lambda = 380$ W/mK for copper thermal conductivity, L_{i-j} is the axial distance from thermocouple i to j. The wall surface temperature T_w is obtained by extending the linear temperature distribution of $T_1 - T_3$ to the surface location. The wall subcooling of the test surface is $\Delta T = T_s - T_w$, where T_s is the saturation vapor temperature. Condensation heat transfer coefficient is calculated as

$$h = \frac{q}{\Delta T} = \frac{q}{T_s - T_w} \tag{2}$$

The maximum uncertainties of heat fluxes and heat transfer coefficients are 6.4% and 10.5%, respectively.

2.4. Calibration experiment

The calibration test was performed on SCS behaving filmwise condensation. In 1916, Nusselt gave a theoretical expression of filmwise condensation heat transfer coefficient on an infinity surface [29]. It should be noted that our test surface is a 30.0 mm diameter circular surface. In 1984, O'Neill and Westwater developed filmwise condensation heat transfer coefficient for a circular surface [3]:

$$h_{\text{Nusselt}} = 0.83403\left(\frac{9.81\lambda_l^3\rho_l^2 h_{lv}}{0.0125\mu_l\Delta T}\right)^{0.25} \tag{3}$$

where λ_l, ρ_l and μ_l are thermal conductivity, density and viscosity of liquid, respectively, h_{lv} is the latent heat of evaporation. Fig. 2b shows reasonable agreement between our measured condensation heat transfer coefficients and predicted values by Eq. (3), with the average error of −12.09%, average absolute error of 12.13% and standard deviation of 8.50%. The measured values are slightly larger than the predicted values. This is because our experiment was performed in a low vapor velocity environment but the theory was developed with zero shear force at vapor-liquid interface. Fig. 2 demonstrates the reliability of our experiment.

3. Results and discussion

3.1. Condensation heat transfer on NGS and SSML

Our experiment lasted two weeks, one week for NGS and one week for SSML. The experiment was continuously running for 12 h every day. Condensation heat transfer coefficients and high speed images for side view were collected simultaneously during initial two-hours of operation in each day.

Fig. 3 shows heat transfer performance for fresh NGS. Two regimes of heat transfer are identified, which are interfaced at wall subcooling of 3.0 °C. The low subcooling regime results in sharp decrease of condensation heat transfer coefficients with increases of wall subcoolings. Condensate droplets observed on the surface are very small having the radii range of ~10 μm, due to the droplet coalescence-induced-jumping mode. When neighboring droplets contact with each other, the merged droplet jumps out of the surface (see Fig. 3a and Supporting Video 1). At the wall supercooling of 3.0 °C, the droplet detachment mode is switched from jumping to rolling (see Fig. 3b and Supporting Video 2). The high subcooling regime yields quasi-constant condensation heat transfer coefficients versus wall subcoolings. Here, droplets detach the surface in rolling mode and droplets remaining on the surface behave the radii range of ~100 μm (see Fig. 3c and Supporting Video 3). By comparing Figs. 2b and 3d, fresh NGS promotes condensation heat transfer coefficients which are 4–5 times of those on SCS.

A major concern of DWC is the occurrence of flooding. The liquid population on the surface is balanced by droplet detachment rate and droplet growth rate. If the droplet detachment rate is larger than the droplet growth rate, liquid cannot be accumulated on the surface to avoid flooding. On the contrary, if the detachment rate is slower than the growth rate, flooding occurs. Because the wall subcooling plays an important role in determining the droplet growth rate, the onset of flooding is strongly dependent on wall subcooling. In other words, the onset of flooding requires a sufficient wall subcooling. Wen et al. [30] reported that the necessary

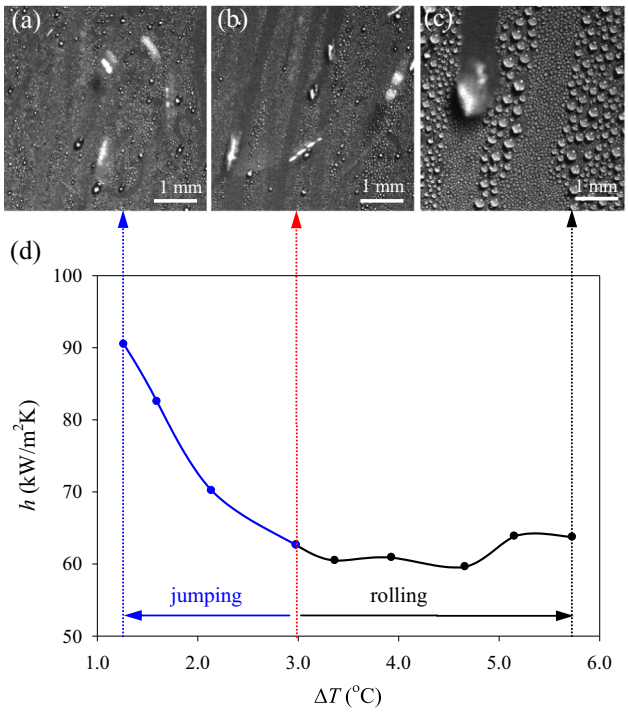

Fig. 3. Side view images and heat transfer coefficients on fresh nanograsses surface (data collected during initial two hours of operation on the first day).

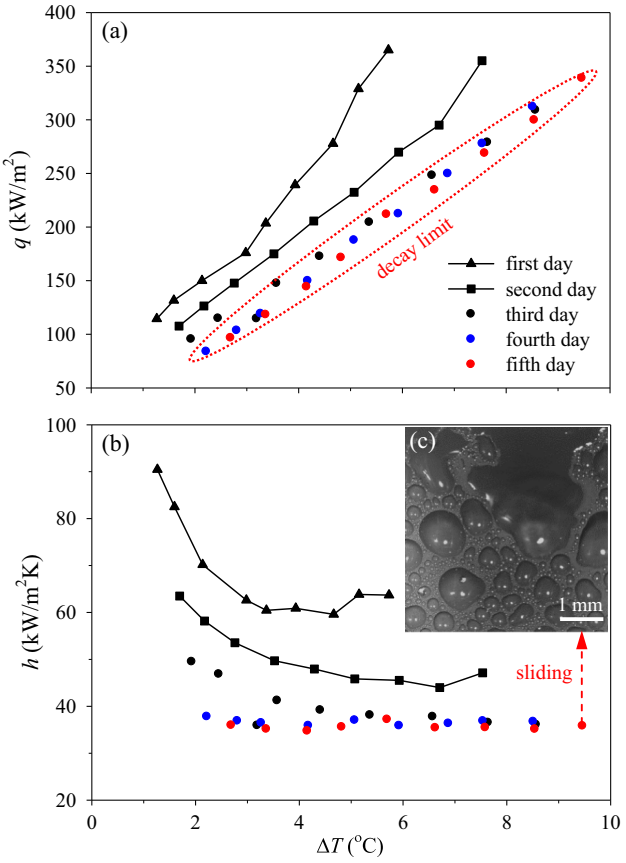

Fig. 4. The decayed condensation heat transfer performance of NGS for one-week operation.

wall subcooling is 21.0 °C. Our experiment had the maximum wall subcooling of 5.7 °C, which is below the wall subcooling limit. Thus, flooding was not observed.

Fig. 4 shows the long-term performance on NGS for five days of operation. Condensation heat fluxes and heat transfer coefficients are decreased from first day to third day, but they approach stable limit values after three days of operation. Condensation heat transfer coefficients after three days of operation are 60% of those on the fresh surface. Droplet removal mechanisms are changed from jumping at low wall subcooling and rolling at high wall subcooling to sliding over the entire wall subcooling range of 1–10 °C (see Fig. 4c and Supporting Video 4). Once the limit values are reached, heat transfer coefficients are almost constant versus wall subcoolings, and heat fluxes behave linear relationship with respect to wall subcoolings. Even though heat transfer is deteriorated for long-term operation, dropwise condensation is still kept and the decayed limit of heat transfer coefficients is ~2 times of those for filmwise condensation on SCS. (see Figs. 4b and 2b).

Most dropwise condensation experiments were performed on fresh nanostructure surface [31]. Very few studies are reported for decayed heat transfer in literature. Torresin et al. [32] reported the decayed condensation on nanostructure surface for long-term operation. Here, we measured condensation heat transfer performance on NGS and analyzed the reason of decayed heat transfer for long-term operation, including observations of droplet detachment mode on fresh surface and the surface after several days of operation, identification of nanostructures for fresh surface and used surface by SEM images, and the proposed nanostructure failure mechanisms. Theoretical analysis regarding the nanostructure failure is presented in Ref. [25].

Droplet detachment mode is important for dropwise condensation. In order to reach high resolution images for droplet dynamics, the optical lens should approach the test surface. However, the optical-lens cannot be inserted inside the condensing chamber. Thus, the visualization experiment for droplet dynamics was performed in a wet air environment. The test surfaces include fresh NGS and NGS after one-week pure vapor condensation in condensing chamber. The experiment setup for humid air condensation is described in our previous work [33,34]. The test was performed at the environment temperature T_e = 26.0 °C, humidity RH = 40%, and surface temperature T_w = 1.0 °C.

On fresh NGS, droplet detachment behaves coalescence-induced-jumping (see Fig. 5a–b for consecutive images at different time and dynamic movies in Supporting Videos 5–7). The observed phenomenon in wet air environment is related to that in pure vapor condensation at low wall subcooling referring to Fig. 3a. Fig. 5c shows the merged droplet trajectory after the coalescence-induced-jumping. On used NGS, the situation is changed compared with that on fresh NGS. The merged droplet adheres on the surface until it becomes large enough by "swallowing" more neighboring droplets to initiate shedding motion along the surface (see Fig. 6 and Supporting Videos 8–10). This droplet motion in wet air environment corresponds to that for pure vapor condensation after several days of operation referring to Fig. 4c.

The decayed heat transfer and changed droplet detachment mode indicate that something happens on nanostructure surface for long-term operation. The nanograss consists of two materials: copper oxide (CuO) as core material and polymer as coating material. CuO is hydrophilic, but polymer is hydrophobic. Here, the phenomenon is examined if the polymer coating layer is broken, under which CuO is exposed to decrease the energy barrier for drop nucleation. The nano-grasses spacing will be filled with liquid to yield Wenzel state of droplet, deterring droplet detachment to degrade heat transfer. Thus, it is necessary to examine if the coating layer is spoiled. Usually, the element analysis can be performed using energy dispersive X-ray spectroscopy (EDX) and X-ray photoelectron spectroscopy (XPS). EDS requires a coating layer thickness of at least 1–2 μm. Our NGS surface has a ~1 nm polymer

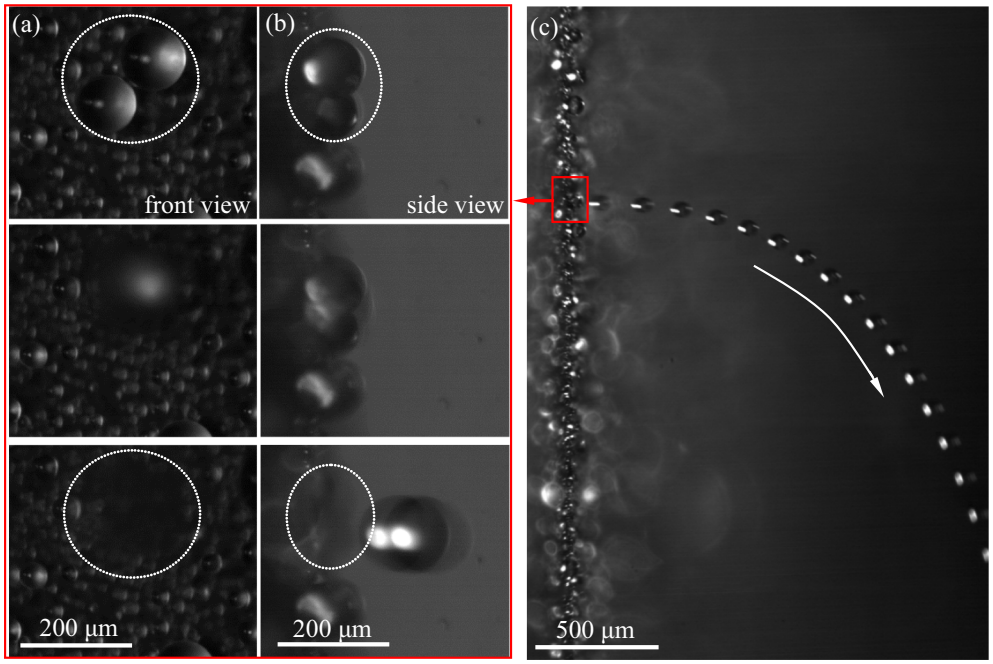

Fig. 5. Coalescence induced jumping on fresh NGS in wet air with T_e = 26.0 °C, RH = 40% and T_w = 1.0 °C (a: front view; b: side view; c: trajectory of merged droplet after jumping).

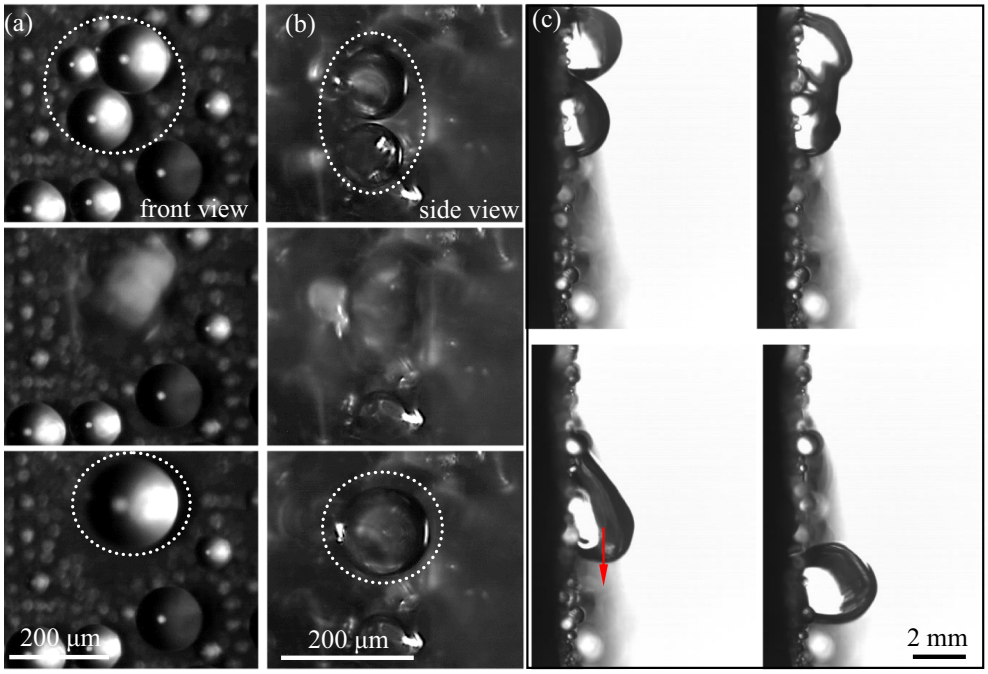

Fig. 6. Droplet shedding on NGS after one-week operation, noting pictures taken in wet air with T_e = 26.0 °C, RH = 40% and T_w = 1.0 °C (a: front view; b: side view; c: detachment progress).

layer thickness, which is significantly smaller than the EDX measurement limit. On other hand, XPS only analyzes the element for smooth surface. Our superhydrophobic surface has nano-scale roughness, which is not suitable to be measured by XPS. Instead, a separate DWC experiments on single-molecule-layer of polymer surface (SSML) was performed for one-week to clarify if the polymer layer on nanograsses is broken. The surface is smooth without nanostructure. The heat fluxes and condensation heat transfer coefficients show no difference during the five days of operation (see Fig. 7). The stable performance of smooth polymer surface verifies the completeness of nanograsses polymer layer, indirectly.

The SEM images and wetting parameters are examined for both NGS and SSML. Data are provided not only before condensation experiment, but also after condensation experiment five days later. The SEM images show no difference between fresh SSML and used SSML (see Fig. 8a–b). The equilibrium contact angle is $\theta = 110.0 \pm 1.8°$. The advancing and receding contact angles are $\theta_a = 120.6 \pm 1.6°$ and $\theta_r = 105.4 \pm 2.5°$, yielding the contact angle

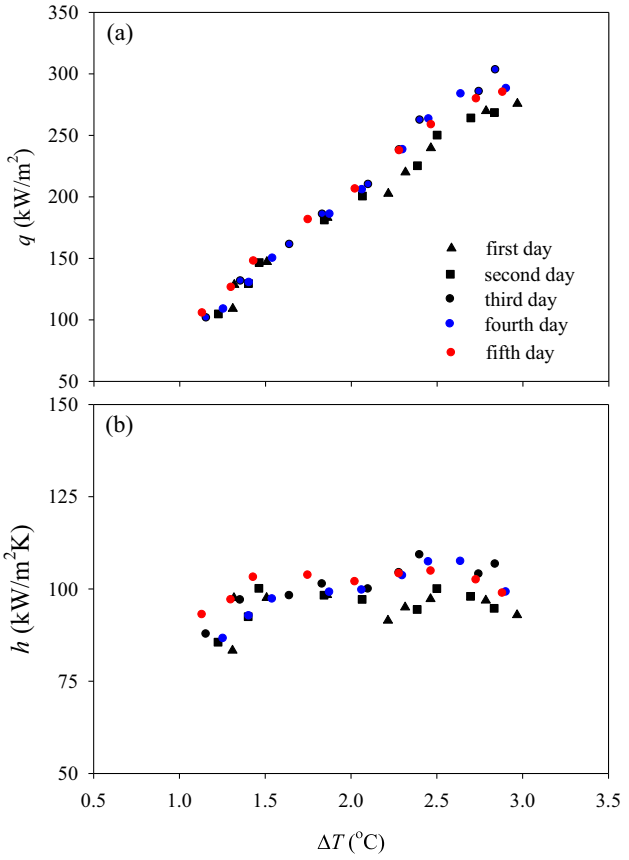

Fig. 7. The stable condensation heat transfer on smooth single-molecule-layer of polymer surface.

hysteresis of $\Omega = \cos\theta_r - \cos\theta_a = 0.241$, where the subscript a and r mean advancing and receding, respectively. The SEM images and contact angle measurement further verify the polymer layer robustness. The polymer layer growing on a copper substrate involves two steps. The first step is the hydration of 1H, 1H, 2H, 2H-perfluorooctyltriethoxysilane polymer to expose –OH bond. The second step is the dehydration synthesis to combine neighboring polymer chains and grow these polymer chains on the copper substrate. The growing process takes place in chain height direction. In summary, polymer macromolecules are bonded with copper atoms via chemical bond, which is solid.

The situation is changed for NGS. Fig. 8c–d for fresh NGS and Fig. 8e–f for used NGS are paid attention. For fresh NGS, nanograsses are densely populated on copper substrate. The statistic analysis gave an average distance between neighboring nanowires of $L_n = 800$ nm, a nanowire diameter of $d_n = 200$ nm and a height of $\delta_n = 3$–4 μm. The wetting parameters are $\theta = 152.0 \pm 1.6°$, $\theta_a = 153.8 \pm 2.2°$ and $\theta_r = 149.6 \pm 3.2°$. The fresh NGS is superhydrophobic to have a rolling angle $RA < 2°$ and a contact angle hysteresis $\Omega = 0.035$. Alternatively, the used NGS not only changed equilibrium contact angle to be 148°, but also changed the surface to be high adhesion. The used NGS cannot repel a droplet even when the droplet is under the surface. The collapse of nanograsses occurs and some nanowires are directly observed to be broken (see Fig. 8e–f). Our observations in nanoscale conclude that the collapse and breakage of nanograsses are the major reason to deteriorate condensation heat transfer.

Based on our SEM measurement, the long-term operation decreases the nano-porous layer roughness and increases the nanowires spacing distance L_n. There are three negative effects of the nanostructure failure on heat transfer. First, the number of drop nucleation sites is decreased due to the decreased nano-porous layer roughness. Second, when L_n is increased, a droplet prefers Wenzel state and sliding detachment mode, making it difficult to depart. Third, the thermal conduction resistance of the nano-porous layer is increased to worsen heat transfer, due to the replacement of nano-grasses by the penetration liquid. This negative contribution is strong due to much smaller thermal conductivities of liquid than solid. The detailed theoretical modeling and quantitative description can be found in Ref. [25].

The heat transfer coefficients of fresh NGS and SSML are re-examined together with the analysis of droplets covering area on the surface (see Fig. 9). The droplet detachment mode influences droplet sizes on the surface to affect condensation heat transfer coefficients. Droplets patterns are significantly different on the two surfaces: (1) NGS repels droplets in jumping mode at low wall subcoolings $\Delta T < 3.0$ °C and rolling mode at high wall subcoolings $\Delta T > 3.0$ °C (see Fig. 3a–c and Supporting Videos 1–3 for NGS), but SSML detaches droplets in sliding mode (see Fig. 9b and Supporting Video 11). (2) Droplets on NGS are one to two orders of magnitude smaller than those on SSML. According to Refs. [35,36], NGS should have higher heat transfer coefficients than SSML due to smaller thermal resistance induced by smaller droplets. This logical inference is against our measured heat transfer results, stating lower heat transfer coefficients of NGS compared to SSML. Our experimental finding concludes the competition of thermal resistances above solid surface and inside nano-porous, playing an important role in determining the overall heat transfer coefficient.

As mentioned in Introduction, DWC on superhydrophobic surface involves various process in multi-time-length-scales: droplet nucleation, growth and detachment, which are influenced by contact angle, contact angle hysteresis and wetting morphology. These processes are couple with each other to make the problem very complicated. Regarding the droplet nucleation, the nanostructure surface obviously increases the number of nucleation sites N_c, which is a positive contribution to heat transfer. Ref. [6] noted that N_c of NGS can be f times of that on smooth surface, where f is the surface roughness. Nanostructure surface decreases the contact angle hysteresis, which is helpful for droplet detachment. Thus, the droplet sizes can be reduced on the surface. Nanostructure surface also raises the contact angle. The increased contact angle is useful to keep jumping or rolling mode, promoting the droplet detachment, which is similar to the effect of reduced contact angle hysteresis. On the other hand, the increased contact angle reduces the contact area between droplet and solid substrate, decreasing the single droplet heat transfer rate, which should be a negative contribution to heat transfer.

One shall remember that nanostructure surface may change Cassie state to Wenzel or partial Wenzel state. The nano-pillars spacing may be occupied by either vapor or liquid. Because thermal conductivities of the fluid phase are smaller than that of solid, the nanostructure surface induces an additional thermal resistance underneath the bulk droplet, which is a negative contribution to heat transfer. The overall thermal performance is a summary of these positive and negative effects. The positive and negative effects of nanostructures will be theoretically investigated in Ref. [25].

3.2. Mechanisms for nanograsses failure

Condensation on superhydrophobic nanostructure surface is complicated, involving several time/length scales interaction between nanostructure and fluid phase. The in-situ-measurement of condensation can only be performed in a strict environment such as vacuum pressure at this stage. The in-situ-measurement of nanostructure failure is a challenge. Here, three mechanisms are proposed to explain the collapse or breakage of nanograsses.

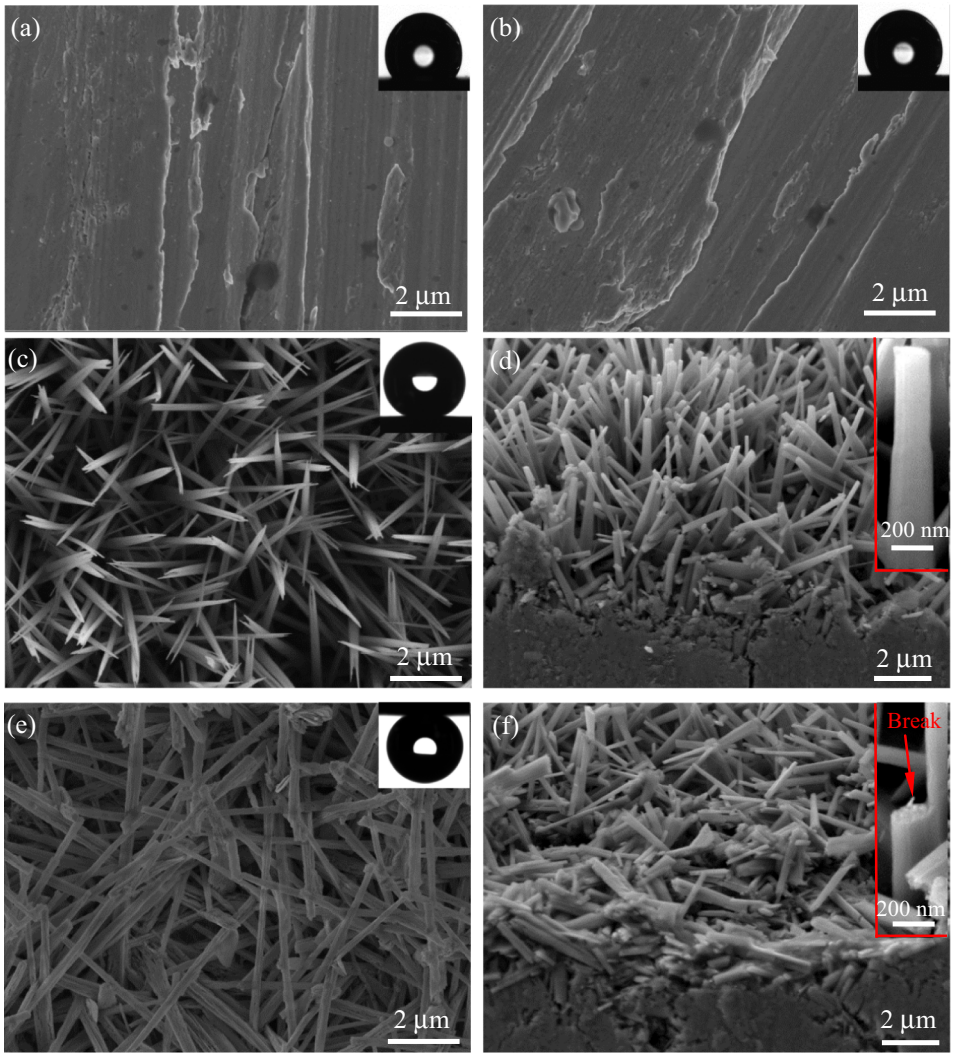

Fig. 8. NGS and SSML Images (a: fresh SSML, *CA* = 110.0°; b: SSML after one-week operation, *CA* = 110.4°; c: top view of fresh NGS, *CA* = 152.0°, *RA* < 2°; d: side view of fresh NGS, nanograss diameter ~200 nm, height ~4 μm; e: top view of NGS after one-week operation, CA = 148.0°, high adhesion; f: side view of NGS after one-week operation).

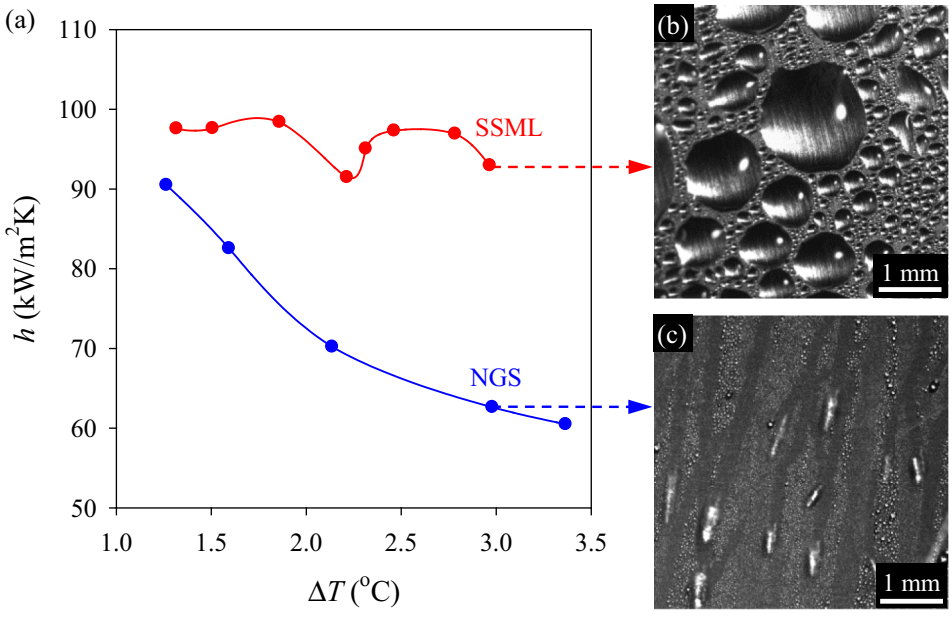

Fig. 9. Condensation heat transfer coefficients on fresh NGS and SSML (a: heat transfer coefficients; b: droplets pattern on SSML; c: droplets pattern on NGS).

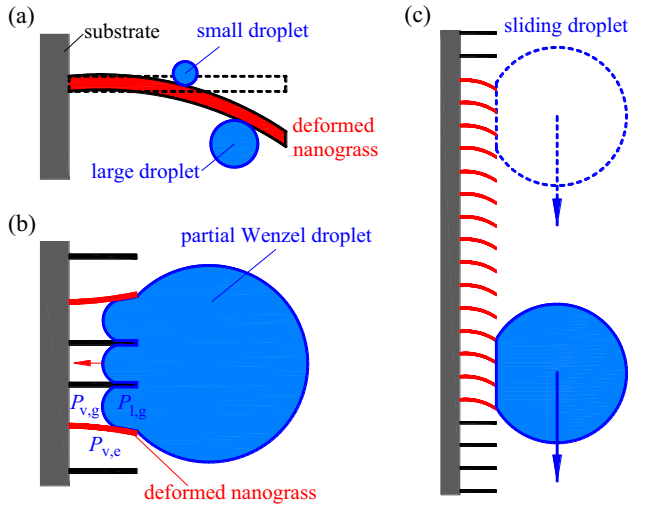

Fig. 10. Three failure mechanisms of NGS (a: droplet nucleation, growth and transport induced failure; b: droplet moving contact line induced failure; c: Bulk drop removal induced failure).

Nanodrop nucleation, growth and transport induced failure (see Fig. 10a): Nanodroplets are nucleating, growing and transporting in nanowires cavities. The spatially populated nanodrops with different sizes apply mechanical stress on nanowires to deform nanowires. The changed nanodrops sizes and locations induce the alternating stress to nanowires. The nanowires may collapse due to the applied fatigue stress.

Nanodrop moving contact line induced failure (see Fig. 10b): At partial Wenzel state, droplet partially penetrates nanostructure gaps to form a set of curved liquid-vapor interfaces. The Laplace pressure difference is $P_{l,g} - P_{v,g} = 2\sigma/r_{lg}$, where r_{lg} is the curvature radius of the liquid-vapor interface inside nano-grasses. The magnitude of r_{lg} is scaled by $\sim L_n$ in nanoscale to cause $P_{l,g} \gg P_{v,g}$. Vapor is connected inside nano-gaps between the nano-grasses supporting droplet and not supporting droplet, yielding $P_{v,g} = P_{v,e}$. This analysis causes $P_{l,g} \gg P_{v,e}$ to significantly deform the nano-grass near three-phase contact line.

Bulk drop removal induced failure (see Fig. 10c): When a droplet of 10 μm–1 mm size slides or rolls on nanostructure surface, each nanowire underneath the droplet sustains part of the force or torque induced by the large drop. As a cantilever beam extended from copper substrate, the nanowire may be failure due to the fatigue stress induced by periodic droplet movement. The nanostructure failure needs further experimental and theoretical investigations, opening a new research field of nanoscale fluid-wall interaction.

4. Conclusions

Two regimes of heat transfer are found on fresh NGS. The low wall subcooling $\Delta T < 3.0$ °C regime has larger heat transfer coefficients, which are sharply decreased with increase of subcoolings. The coalescence-induced-jumping keeps smaller droplets on surface. The high subcooling $\Delta T > 3.0$ °C regime holds constant heat transfer coefficients having rolling detachment mode.

The one-week operation apparently worsens heat transfer. The condensation heat transfer coefficients are decreased from first to third day, but approach limit value since the third day. The long-term operation changes droplet detachment mode to sliding. Running similar experiment on a smooth polymer surface indicates no failure of the polymer layer on nanograss surface.

SEM images directly show the collapse and breakage of nanograsses after one-week operation. The fresh surface is superhydrophobic with low adhesion, but the used surface is high adhesion. The long-term operation apparently decreases nanostructure roughness and changes surface topology. Three mechanisms are proposed to explain the nanograsses failure.

The fresh NGS has smaller droplet departure size due to jumping or rolling mode, but has lower heat transfer coefficients compared to SSML, indicating positive and negative contributions of nanostructure on condensation heat transfer.

Conflict of Interest

The authors declared that there is no conflict of interest.

Acknowledgements

The authors thank for the funding support by National Natural Science Foundation of China (51436004), China Postdoctoral Science Foundation (2017M620712) and Fundamental Research Funds for the Central Universities (JB2014005).

Appendix A. Supplementary material

Supplementary data associated with this article can be found, in the online version, at https://doi.org/10.1016/j.ijheatmasstransfer.2018.09.100.

References

[1] E. Schmidt, W. Schurig, W. Sellschopp, Versuche über die Kondensation von Wasserdampf in Film-und Tropfenform, Technische Mechanik Thermodynamik 1 (2) (1930) 53–63.
[2] D.W. Woodruff, J.W. Westwater, Steam condensation on electroplated gold: Effect of plating thickness, Int. J. Heat Mass Transf. 22 (4) (1979) 629–632.
[3] G.A. O'Neill, J.W. Westwater, Dropwise condensation of steam on electroplated silver surfaces, Int. J. Heat Mass Transf. 27 (9) (1984) 1539–1549.
[4] D.W. Woodruff, J.W. Westwater, Steam condensation on various gold surfaces, J. Heat Transfer 103 (4) (1981) 685–692.
[5] B.S. Sikarwar, N.K. Battoo, S. Khandekar, K. Muralidhar, Dropwise condensation underneath chemically textured surfaces: simulation and experiments, J. Heat Transfer 133 (2) (2011) 216–226.
[6] S. Khandekar, K. Muralidhar, Dropwise Condensation on Inclined Textured Surfaces, Springer, New York, 2014.
[7] S. Anand, A.T. Paxson, R. Dhiman, J.D. Smith, K.K. Varanasi, Enhanced condensation on lubricant-impregnated nanotextured surfaces, ACS Nano 6 (11) (2012) 10122–10129.
[8] R. Xiao, N. Miljkovic, R. Enright, E.N. Wang, Immersion condensation on oil-infused heterogeneous surfaces for enhanced heat transfer, Sci. Rep. 3 (2013) 1988.
[9] S. Lee, K. Cheng, V. Palmre, M.D.M.H. Bhuiya, K.J. Kim, B.J. Zhang, H. Yoon, Heat transfer measurement during dropwise condensation using micro/nano-scale porous surface, Int. J. Heat Mass Transf. 65 (2013) 619–626.
[10] J.R. Lara, M.T. Holtzapple, Experimental investigation of dropwise condensation on hydrophobic heat exchangers. Part II: Effect of coatings and surface geometry, Desalination 280 (2011) 363–369.
[11] Q. Zhao, D.C. Zhang, J.F. Lin, G.M. Wang, Dropwise condensation on L-B film surface, Chem. Eng. Process. Process Intensif. 35 (1996) 473–477.
[12] S.N. Aksan, J.W. Rose, Dropwise condensation—The effect of thermal properties of the condenser material, Int. J. Heat Mass Transf. 16 (1973) 461–467.
[13] J. Rafiee, X. Mi, H. Gullapalli, A.V. Thomas, F. Yavari, Y.F. Shi, P.M. Ajayan, N.A. Koratkar, Wetting transparency of grapheme, Nat. Mater. 11 (2012) 217–222.
[14] G. Azimi, R. Dhiman, H.M. Kwon, A.T. Paxson, K.K. Varanasi, Hydrophobicity of rare-earth oxide ceramics, Nat. Mater. 12 (2013) 315–320.
[15] N. Miljkovic, R. Enright, Y. Nam, K. Lopez, N. Dou, J. Sack, E.N. Wang, Jumping-droplet-enhanced condensation on scalable superhydrophobic nanostructured surfaces, Nano Lett. 13 (2013) 179–187.
[16] J.B. Boreyko, C.H. Chen, Self-Propelled dropwise condensate on superhydrophobic surfaces, Phys. Rev. Lett. 103 (2019) 184501.
[17] X.J. Gong, X.F. Gao, L. Jiang, Recent progress in bionic condensate microdrop self-propelling surfaces, Adv. Mater. 29 (45) (2017) 1703002.
[18] J. Zhu, Y.T. Luo, J. Tian, J. Li, X.F. Gao, Clustered ribbed-nanoneedle structured copper surfaces with high-efficiency dropwise condensation heat transfer performance, ACS Appl. Mater. Interfaces 7 (2015) 10660–10665.
[19] H. Kim, Y. Nam, Condensation behaviors and resulting heat transfer performance of nano-engineered copper surfaces, Int. J. Heat Mass Transf. 93 (2016) 286–292.

[20] N. Miljkovic, R. Enright, E.N. Wang, Effect of droplet morphology on growth dynamics and heat transfer during condensation on superhydrophobic nanostructured surfaces, ACS Nano 6 (2) (2012) 1776–1785.
[21] B.J. Zhang, C. Kuok, K.J. Kim, T. Hwang, H. Yoon, Dropwise steam condensation on various hydrophobic surfaces: Polyphenylene sulfide (PPS), polytetrafluoroethylene (PTFE), and self-assembled micro/nano silver (SAMS), Int. J. Heat Mass Transf. 89 (2015) 353–358.
[22] Z. Lan, X.H. Ma, S.F. Wang, M.Z. Wang, X.N. Li, Effects of surface free energy and nanostructures on dropwise condensation, Chem. Eng. J. 156 (3) (2010) 546–552.
[23] X.H. Ma, S.F. Wang, Z. Lan, A. Wang, B.L. Peng. Dropwise condensation heat transfer on superhydrophobic surface in the presence of non-condensable gas, in: Proceedings of the 14th International Heat Transfer Conference, 2010, pp. 71–79.
[24] H.W. Hu, G.H. Tang, D. Niu, Experimental investigation of condensation heat transfer on hybrid wettability finned tube with large amount of noncondensable gas, Int. J. Heat Mass Transf. 85 (2015) 513–523.
[25] J. Xie, J.L. Xu, W. Shang, K. Zhang, Dropwise condensation on superhydrophobic nanostructure surface, Part II: Mathematical model, Int. J. Heat Mass Transf. 127 (2018) 1170–1187.
[26] D.W. Tanner, D. Pope, C.J. Potter, D. West, Heat transfer in dropwise condensation at low steam pressures in the absence and presence of non-condensable gas, Int. J. Heat Mass Transf. 11 (1968) 181–190.
[27] J. Feng, Z.Q. Qin, S.H. Yao, Factors affecting the spontaneous motion of condensate drops on superhydrophobic copper surfaces, Langmuir 28 (2012) 6067–6075.
[28] X.H. Chen, L.H. Kong, D. Dong, G.B. Yang, L.G. Yu, J.M. Chen, P.Y. Zhang, Fabrication of functionalized copper compound hierarchical structure with bionic superhydrophobic properties, J. Phys. Chem. C 113 (14) (2009) 5396–5401.
[29] W. Nusselt, Die Oberflächenkondensation Des Wasserdampfes, Zeitschrift des Vereines deutscher ingenieure 60 (1916) 541–569.
[30] R.F. Wen, S.S. Xu, X.H. Ma, Y.C. Lee, R.G. Yang, Three-dimensional superhydrophobic nanowire networks for enhancing condensation heat transfer, Joule 2 (2) (2018) 269–279.
[31] H.J. Cho, D.J. Preston, Y.Y. Zhu, E.N. Wang, Nanoengineered materials for liquid-vapour phase-change heat transfer, Nat. Rev. Mater. 2 (2016) 16092.
[32] D. Torresin, M.K. Tiwari, D. Del Col, D. Poulikakos, Flow condensation on copper-based nanotextured superhydrophobic surfaces, Langmuir 29 (2013) 840–848.
[33] J. Xie, J.L. Xu, Q. Liu, X. Li, Coupling diffusion welding technique and mesh screen creates heterogeneous metal surface for droplets array, Adv. Mater. Interfaces 4 (23) (2017) 1700684.
[34] J. Xie, J.L. Xu, X.T. He, Q. Liu, Large scale generation of micro-droplet array by vapor condensation on mesh screen piece, Sci. Rep. 7 (2017) 39932.
[35] S. Lee, H.K. Yoon, K.J. Kim, S.W. Kim, M. Kennedy, B.J. Zhang, A dropwise condensation model using a nano-scale, pin structured surface, Int. J. Heat Mass Transf. 60 (2013) 664–671.
[36] B.J. Qi, J.J. Wei, L. Zhang, H. Xu, A fractal dropwise condensation heat transfer model including the effects of contact angle and drop size distribution, Int. J. Heat Mass Transf. 83 (2015) 259–272.